Hindawi
International Journal of Antennas and Propagation
Volume 2018, Article ID 1692018, 9 pages
https://doi.org/10.1155/2018/1692018

Research Article

A Novel Wideband Circularly Polarized Antenna for RF Energy Harvesting in Wireless Sensor Nodes

Nhu Huan Nguyen,[1,2] Thi Duyen Bui,[1] Anh Dung Le,[1,2] Anh Duc Pham,[1] Thanh Tung Nguyen,[3] Quoc Cuong Nguyen,[1] and Minh Thuy Le[1]

[1]*Department of Instrumentation and Industrial Informatics, School of Electrical Engineering, Hanoi University of Science and Technology, Hanoi 10000, Vietnam*
[2]*University of Grenoble Alpes, Grenoble, France*
[3]*Institute of Materials Science, Vietnam Academy of Science and Technology, Hanoi 10000, Vietnam*

Correspondence should be addressed to Minh Thuy Le; thuy.leminh@hust.edu.vn

Received 16 September 2017; Revised 24 December 2017; Accepted 8 January 2018; Published 11 March 2018

Academic Editor: N. Nasimuddin

A novel wideband circularly polarized antenna array using sequential rotation feeding network is presented in this paper. The proposed antenna array has a relative bandwidth of 38.7% at frequencies from 5.05 GHz to 7.45 GHz with a highest gain of 12 dBi at 6 GHz. A corresponding left-handed metamaterial is designed in order to increase antenna gain without significantly affecting its polarization characteristics. The wideband circularly polarized antenna with 2.4 GHz of bandwidth is a promising solution for wireless communication system such as tracking or wireless energy harvesting from Wi-Fi signal based on IEEE 802.11ac standard or future 5G cellular. A potential application of this antenna as a receiving antenna for RF-DC device to obtain DC power for a wireless sensor node from Wi-Fi signal is shown.

1. Introduction

In the recent years, wireless sensor network (WSN) has attracted the attention in wireless communication domain for monitoring, medical observation, military surveillance, localization, smart home, smart building, and smart city [1]. A common WSN consists of two main parts: (i) a system of wireless sensor nodes attached to nonrechargeable batteries and (ii) a base station. The life cycle of primary batteries becomes the main drawback for wireless sensor nodes where the cost for maintenance and replacement of the batteries is unavoidable. RF energy harvesting or wireless power transfer (WPT) is proposed as a durable power source in WSN [2].

This paper presents an efficient RF energy harvesting solution. The RF energy harvesting cell is often integrated in each self-powered sensor node to convert surrounding RF power into DC power source. Traditional RF harvester includes a receiving antenna, a RF band-pass filter, a matching network, a rectifier with low-pass filter, and a terminal load. The received RF power at the output of antenna is delivered to rectifier through band-pass filter and impedance-matching circuit to be converted into high-efficient DC power as discussed later. The rectenna, sometimes known as rectifying antenna, plays the central role in converting RF power into DC power in RF energy harvesting as well as WPT system, and it has attracted significant attention in the past few years.

Solutions to high conversion efficiency rectenna were reported in [3–8] where the influence of receiving antenna on system performance (in term of conversion efficiency and working distance) has been systematically investigated in [6, 9]. A high-gain antenna is preferred for the longest distance applications while a wideband operation antenna allows multiple frequency channels in order to reduce inter-channel-interference and to receive random RF signals in ambient environment such as GSM 900, GSM 1800,

UMTS, Wi-Fi, and WiMAX. Furthermore, a circularly polarized (CP) antenna is desirable to receive electromagnetic energy from different polarizations to improve the total conversion efficiency. Therefore, a wideband and high-gain CP antenna is a good candidate to collect energy from random polarization at different operating frequencies for RF energy harvesting.

Circularly polarized antennas can be achieved using single-feed or multiple-feed structures. Several antennas for RF energy harvesting have been reported in [10–15]. A multilayer patch antenna with CP performance is presented for energy harvesting application in [10]. The omnidirectional circularly polarized antenna is achieved using the truncation corner topology and multilayer structure antenna. This antenna has 3.6% bandwidth at center frequency of 2.41 GHz (from 2.43 GHz to 2.45 GHz). When this antenna is used as receiving antenna in RF energy harvester, the output voltage at frequency of 2.40 GHz is 255 mV. In [11], an E-shaped slot is investigated along the orthogonal axis of the circular patch to generate CP performance and to improve antenna gain. This antenna has wide-angle CP radiation of 140° with a bandwidth of 3.2% and a gain of more than 5.0 dBic at 2.38 GHz. Four stubs are integrated at four corn of a square patch antenna to have CP performance in [12]. A maximum 10 dB bandwidth of 4.8% at 2.5 GHz is obtained for the asymmetric gap case. The corresponding maximum gain is 4.5 dBic and the average output voltage of 1.5 mV is achieved at different rotation angles. The narrow bandwidth is the disadvantage of CP antennas reported in literature [10–12]. A wideband and high-gain CP antenna is reported in [13]. Circular polarization is generated by cutting a Teo-shaped slot at the square patch radiator while an aperture coupling is used to broaden the bandwidth. A 10 dB bandwidth of 33% (1.89–2.66 GHz) with 3 dB axial ratio (AR) bandwidth of 100 MHz (2.4–2.5 GHz) and maximum gain of 6.8 dBic are achieved at 2.28 GHz and 2.5 GHz, respectively. This antenna has a good performance in term of size, bandwidth, and gain. However, the aperture coupling is a disadvantage in fabrication point of view. In [14], a pair of cross bowtie antennas is used to have wideband CP performance while the antenna gain is improved by a reflector. The obtained 10 dB bandwidth is 38.2% (1.357–1.997 GHz) and total gain is greater than 7.5 dB in operating bandwidth. This 3D structure is complex in fabrication point of view. Substrate integrated waveguide (SIW) technology was reported to realize a very high performance cavity-backed planar antenna array in [15]. Two pairs of rectangular slots are used to have CP while the cavity defines operating bandwidth. A maximum gain of 20.1 dBi at 6.6 GHz and a 10 dB bandwidth of 3.2% (6.52–6.73 GHz) are obtained for a 4×4 antenna array.

In this paper, a novel wideband CP patch antenna using a wideband left-handed metamaterial (WBLHM) substrate to improve the antenna gain is proposed. Both simulated and measured verifications are investigated to highlight its performance. The paper is organized as follows. WBLHM unit cell analytical model is presented in Section 2. Section 3 applies this LHM substrate on a wideband CP antenna array as a high-gain and wideband solution. The demonstration of the complete RF energy harvesting system is presented in Section 4.

2. Novel WBLHM Structure: Modelling and Analysis

2.1. WBLHM Modelling. Left-handed metamaterials are unnatural structures with double negative permittivity and negative permeability (DNG). LHM substrate acts like an electromagnetic lens, thus it is placed above a reference antenna to concentrate the wave out of reference antenna into the perpendicular direction of LHM substrate for increasing antenna gain. In this section, a LHM unit cell is analysed to investigate the operation of the whole periodical structure.

It is known that the negative permeability results from the magnetic response to an external magnetic field while the negative permittivity is due to either a low-frequency plasma behaviour or an electric resonance response [16]. Once the frequency range of negative permittivity and negative permeability overlaps, we can achieve a negative refractive region. This consideration is valid only if the metamaterial (MTM) can be approximated as an effectively homogeneous medium, which means the size of MTM unit cells p must be sufficiently smaller than the guided wavelength λ_g. In most cases, p should be smaller than $\lambda_g/4$ [17]. Smith and coworkers proposed a well-known structure, namely square split ring resonator (SSRR), with dimensions of $8 \times 8\,\text{mm}^2$ ($p \sim \lambda_0/7.5$) in x and y directions, where λ_0 is the wavelength in free space [18, 19]. In their structure, the square split ring leads the negative permeability while the continuous wire causes the negative permittivity [20]. However, the double negative range of this structure and then the negative refractive band are narrow. The WBLHM is obtained by a geometrical transformation from SSRR structure with four top quasi-opened rings and two bottom cross wires. Figure 1 illustrates the proposed WBLHM with defined parameters and its equivalent circuit. The meander line is used for miniaturization purpose in x and y directions. Unit cell is designed with dimensions of $W \times L = 5.5 \times 5.5\,\text{mm}^2$ ($p \sim \lambda_0/9.4$), 20% smaller than a SSRR unit cell. The copper material of strip line is chosen with a thickness of 0.035 mm while the thickness of Rogers RO4003 substrate is $h_s = 0.8$ mm with the relative permittivity, $\varepsilon_r = 3.55$ and $\tan\delta = 0.0027$.

As it can be seen in Figure 1(a), C_t, C_s, and C_m represent the capacitance caused by the asymmetric gap of each unit cell, the capacitance between two layers, and the mutual coupling between two continuous unit cells, respectively. L_t and L_b are the total inductance of the folded line on top layer and the cross line on bottom layer, respectively. The induced electric energy is mostly concentrated between the two gaps spacing by d_g on top layer. The induced magnetic energy is mainly located at the meander line of width d_m. These electromagnetic distributions are shown in Figures 1(a) and 1(b). The capacitance C_t controls the electrical resonance and negative permittivity while the meander line size d_m controls the negative permeability. The effect of d_g and d_m on the epsilon negative bandwidth (ENB) and the mu

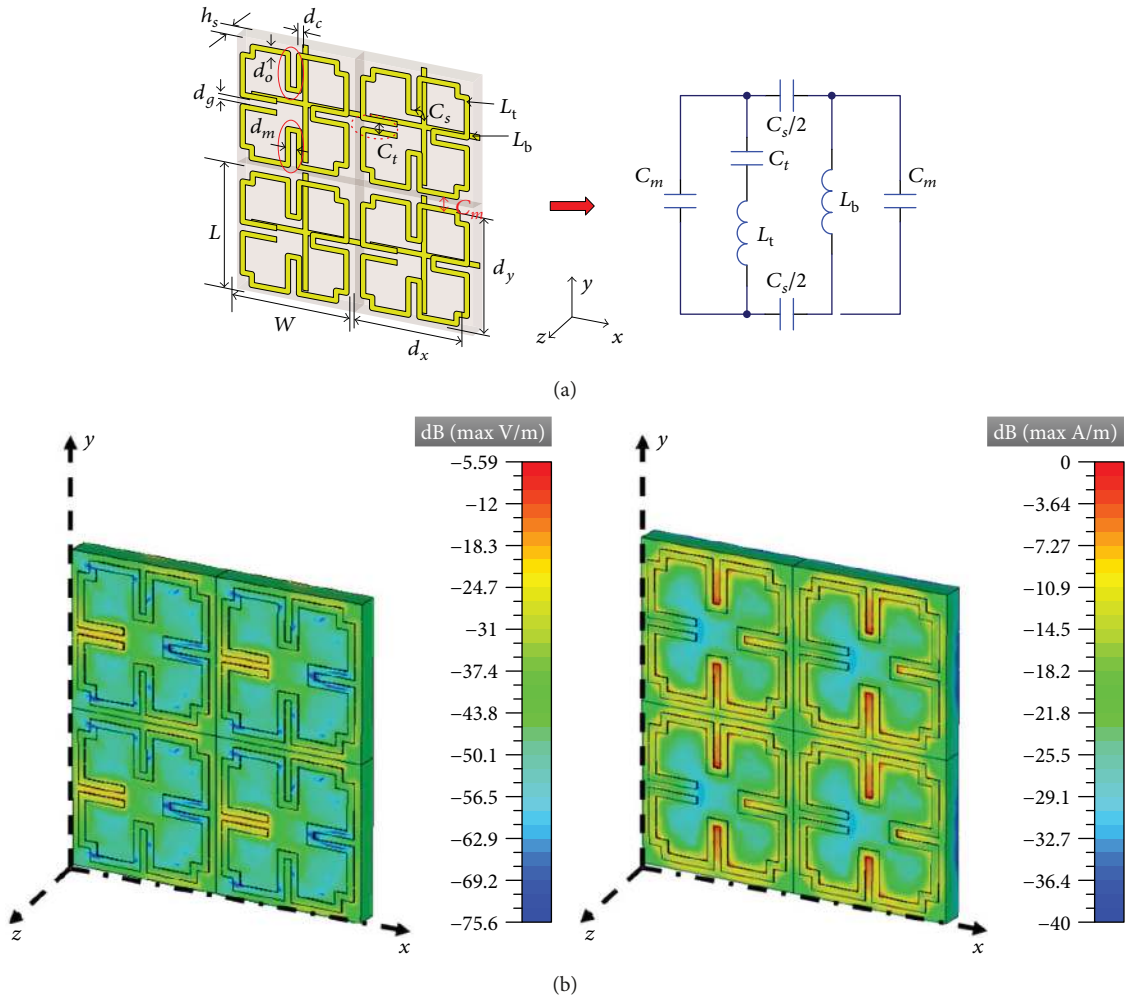

FIGURE 1: (a) WBLHM geometry and equivalent circuit $W = L = 5.5$ mm, $d_x = d_y = 5$ mm, $d_o = 0.25$ mm, $d_g = 0.25$ mm, $d_c = 0.25$ mm, $d_m = 0.25$ mm. (b) Electric field (left) and magnetic field (right) distribution in cross-section view.

TABLE 1: Effect OF d_g on ENB AND M.

Value of d_g (mm)	ENB (GHz)	MNB (GHz)
0.2	3.41	6.3
0.25	3.34	6.47
0.3	3.33	6.22

TABLE 2: Effect of d_m on MNB and ENB.

Value of d_m (mm)	MNB (GHz)	ENB (GHz)
0.2	6.51	3.36
0.25	6.47	3.34
0.3	6.26	3.38

negative bandwidth (MNB) are described in Tables 1 and 2. The proposed unit cell has dimensions $d_g = 0.25$ mm and $d_m = 0.25$ mm for wideband DNG. The geometrical parameters of proposed WBLHM unit cell are shown in Figure 1.

2.2. Wideband Negative Effective Permittivity and Permeability. The permittivity and permeability of a homogeneous medium can be found using the field-averaging method [21–23] or the retrieval scattering parameters [24–26]. In this study, we applied the method proposed by Chen and coworkers. Firstly, the refractive index n and the impedance z are obtained. Then, the effective permittivity and permeability of LHM are directly calculated by using these equations: $\mu = nz$ and $\varepsilon = n/z$. This method has been widely used for determining effective permittivity and permeability. The proposed WBLHM unit cell dimension is smaller than $\lambda_0/4$. Therefore, as mentioned above, the WBLHM can be effectively considered as a homogeneous material at the studied frequencies, and the presented method in [26] is suitable to retrieve the effective permittivity and permeability. The obtained effective permittivity and permeability are negative in a very wide band as in Figure 2. The ENB of 3.34 GHz from 5.27 GHz to 8.61 GHz together with the MNB of 6.47 GHz from 5.34 GHz to 11.81 GHz are obtained for our WBLHM unit cell. This unit cell has wideband DNG from 5.34 GHz to 8.61 GHz.

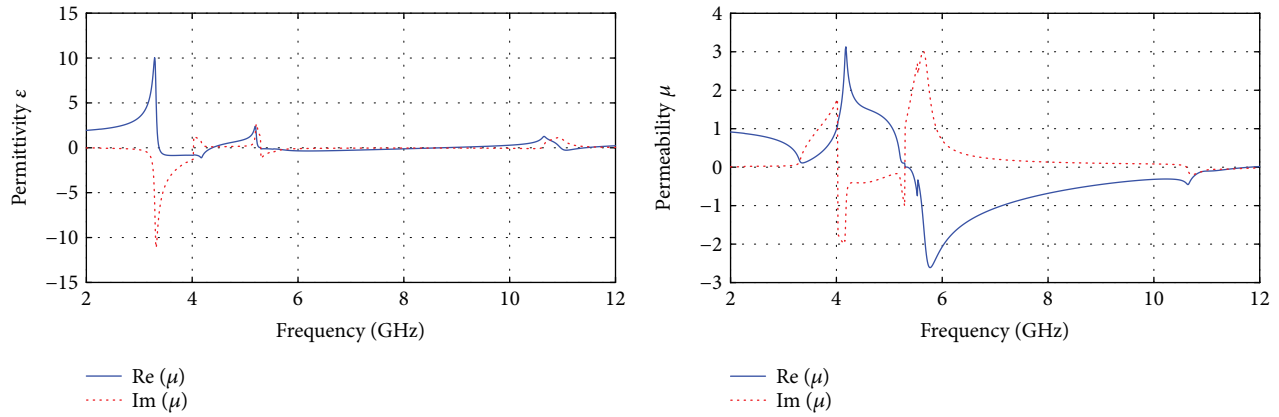

Figure 2: (a) The extracted effective permittivity. (b) The extracted effective permeability.

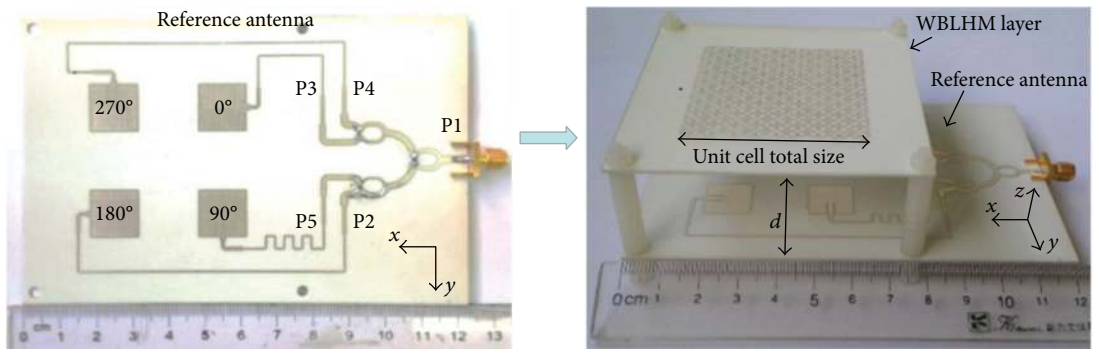

Figure 3: Wideband CP LHM antenna prototype.

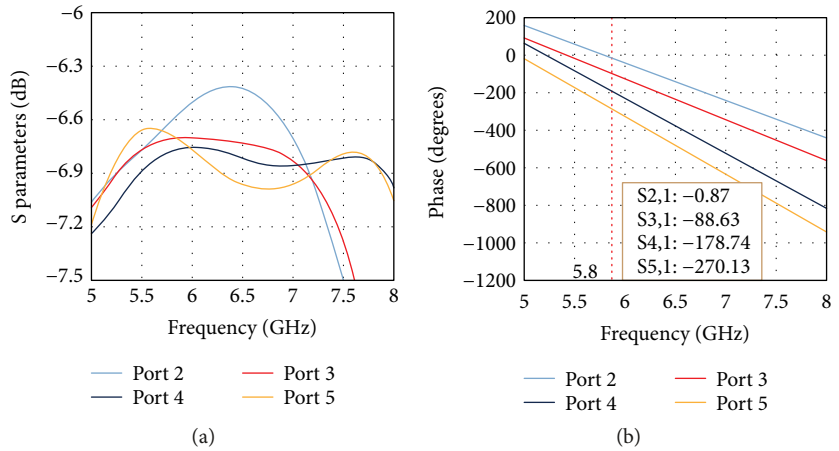

Figure 4: Amplitude (a) and phase (b) distribution of proposed feeding network.

3. WBLHM for Antenna Gain Enhancement: Results and Discussion

3.1. Wideband Circularly Polarized Patch Antenna. The array of 2 × 2 patch elements based on sequential rotation technique that generates an excellent CP over a relatively wide frequency bandwidth is designed as the reference antenna. Figure 3 shows the configuration of four patches with feed phase arranged in 0°, 90°, 180°, and 270°. In sequential rotation technique, the excited amplitudes and phases play an important role to the CP property of the antenna. The excited amplitudes to four elements must be the same power (around −6.7 dB) while the excited phase must be arranged in 0°, 90°, 180°, and 270° at the 5.8 GHz as in Figure 4. The proposed feeding network using Wilkinson power divider [27] excites equal amplitude and phase arranged in 0°, 90°, 180°, and 270° to four patch elements in order to obtain a good axial ratio (AR) over the frequency from 5.52 GHz to

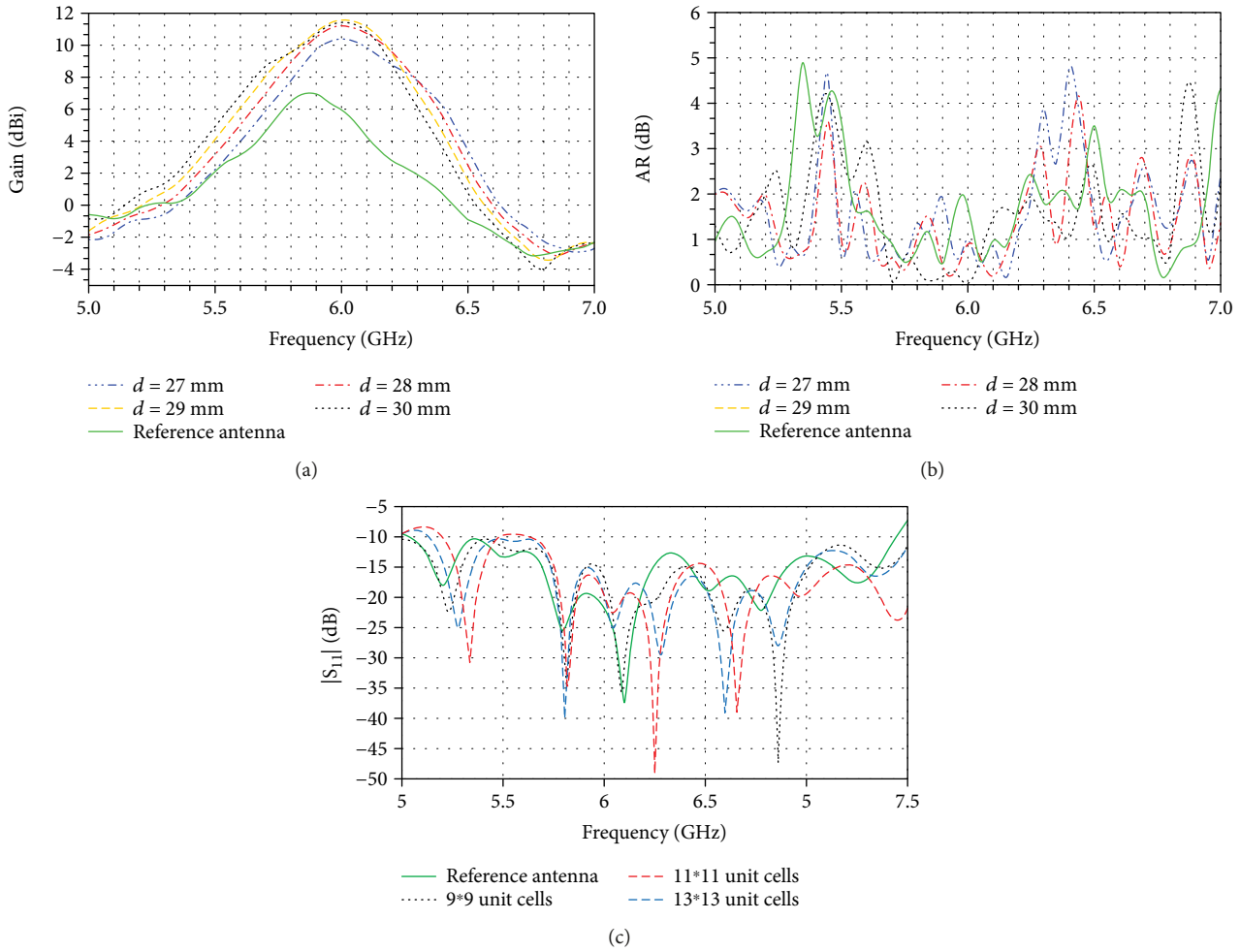

Figure 5: (a) Gain of reference antenna with and without WBLHM layer at different distances d. (b) Axial Ratio (AR) of reference antenna with and without WBLHM layer at different distances d. (c) Reflection coefficient of reference antenna with and without WBLHM layer using various number of unit cells.

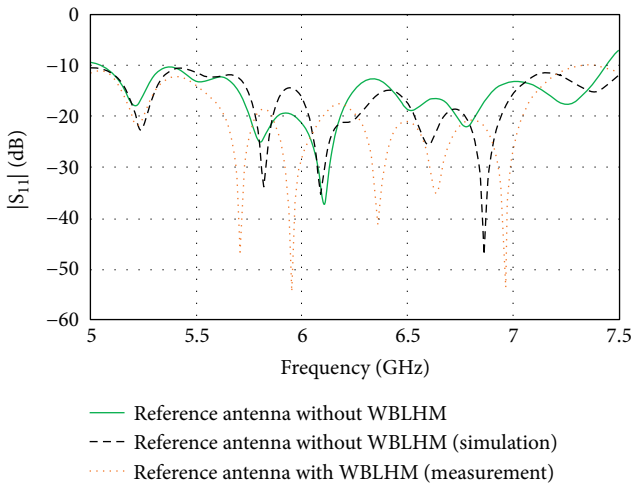

Figure 6: Simulated and measured S_{11} of reference antenna with and without WBLHM layer.

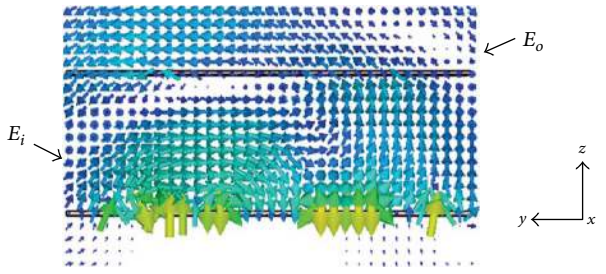

Figure 7: E-field on reference antenna with WBLHM layer.

6.50 GHz as presented in Figure 5(b). The reference antenna has a bandwidth of 2.4 GHz (from 5.05 GHz to 7.45 GHz) with the reflection coefficient $|S_{11}|$ illustrated in Figure 5(c) and the antenna gain is shown in Figure 5(a).

3.2. Antenna Gain Enhancement. The WBLHM substrate is placed above the wideband CP patch antenna at a distance of d as topology in Figure 3 to enhance the antenna gain. This high-gain and wideband CP LHM antenna gain

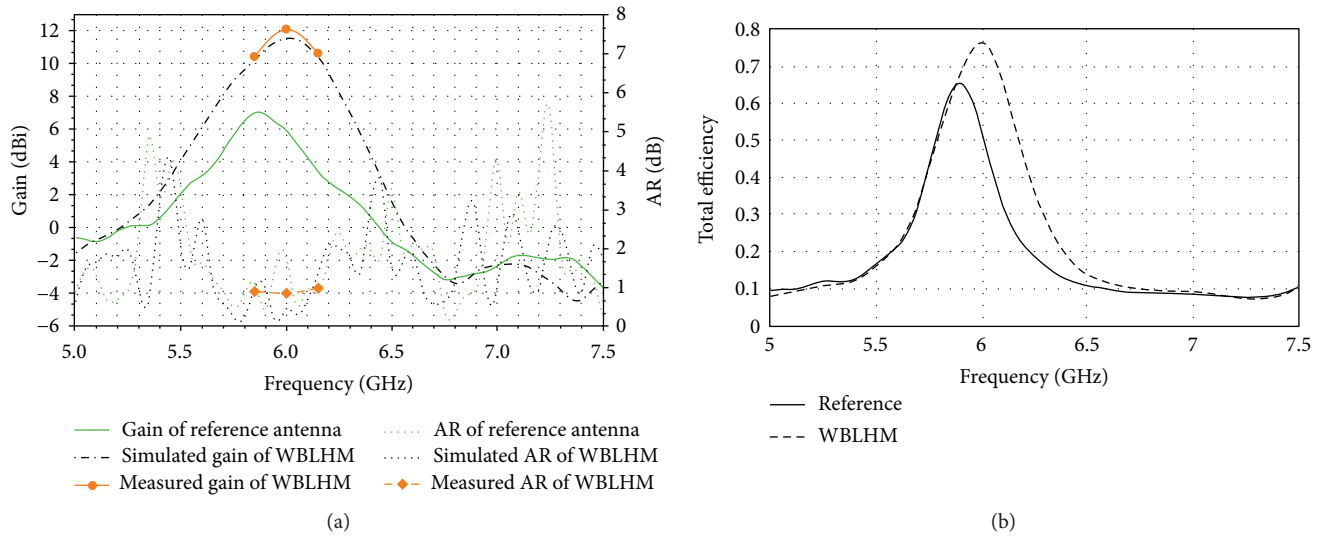

FIGURE 8: (a) Gain and AR of reference antenna and WBLHM antenna at $d = 29$ mm. (b) Total efficiency of reference and WBLHM antenna.

and axial ratio (AR) at different values of d are presented in Figures 5(a) and 5(b).

Some points must be noticed to design a high-gain and wideband CP antenna using WBLHM substrate. Firstly, the distance d between WBLHM layer and the reference antenna is the most affected parameter to AR [28]. In order to reduce the total size of this 3D structure in z direction (as shown in Figure 3), the WBLHM layer needs to be maintained as closely as possible to the reference antenna for a gain enhancement while a good AR is maintained. The optimum value obtained by simulation is $d = 0.56\lambda_0$, which is equivalent to the focal length of WBLHM layer at 5.8 GHz. Secondly, the total size of WBLHM layer (the number of unit cell on WBLHM layer) must be considered to get a homogeneous structure. The radiated electromagnetic of the reference antenna is a power source for WBLHM layer, which is why the proposed WBLHM must cover the radiation beam width of CP reference antenna to get a higher performance. In the experiment, the size is large enough to cover all of radiator patch, not always including the feed line. The distance d is varied at several values around $0.56\lambda_0$ as in Figures 5(a) and 5(b). The bigger total size is, the narrower bandwidth becomes. After considering both gain peak, AR and bandwidth, a distance of $d = 29$ mm, and a total size of $9 * 9$, unit cells are chosen to obtain higher gain and wideband AR. As can be seen in Figure 6, the wideband behaviour is almost unchanged after covering the reference antenna with this WBLHM layer. These effects of the WBLHM are explained in the electric field distribution presented in Figure 7.

The electric field out of wideband LHM layer (E_o) differs from E_i because of the reduction and the phase shift of electric fields according to the distance d and the asymmetric of WBLHM structure. E_o can be represented by E_{ox} and E_{oy} in x and y directions:

$$E_{ox} = E_{ix}.r_x e^{j\varphi_{ox}}$$
$$E_{oy} = E_{iy}.r_y e^{j\varphi_{oy}} \quad (1)$$

for r_x, r_y are the reduction and φ_{ox}, φ_{oy} are the phase shifts of electric fields in x and y directions, respectively. In result, we have the magnitude of electric field are represented as:

$$\mathrm{Mag}(E_{ox}) = E_x.r_x$$
$$\mathrm{Mag}(E_{oy}) = E_y.r_y \quad (2)$$

and the phase shift of electric field:

$$\Delta\varphi = (\varphi_{ix} - \varphi_{iy}) + (\varphi_{ox} - \varphi_{oy}) \quad (3)$$

Because of the asymmetric of WBLHM structure as mentioned in Section 2.1, the electric field passing through this layer has different shifts for both magnitude and phase in x and y directions. For this reason, the CP performance of reference antenna is changed, and the main beam of reference antenna is squinted. However, these changes are not significant, and these results are shown in Figure 8(a). The antenna gain reaches the maximal value of 11.58 dBi (in simulation) and 12 dBi (in measurement) at 6 GHz and is enhanced for the maximal value of 7.02 dBi at 6.15 GHz.

The total efficiency e_0 is a product of three factors: $e_0 = e_r e_c e_d$, where e_r is the reflection efficiency, e_c is the conduction efficiency, and e_d is the dielectric efficiency [29]. Furthermore, $e_{cd} = e_c e_d$ is the antenna radiation efficiency, which relates to the antenna gain and directivity. Because of the effect of WBLHM layer on antenna impedance matching and the variation of electromagnetic field passing through this layer, the total efficiency is a frequency dependent. The total efficiency of reference antenna with WBLHM layer is enhanced over the bandwidth from 5.9 GHz to 7.1 GHz (Figure 8(b)). The simulated and measured radiation patterns of this proposed antenna at 5.82 GHz are illustrated in Figure 9(a) with 10.7 dBi of gain peak and 1 dB of AR showing a good circular polarization.

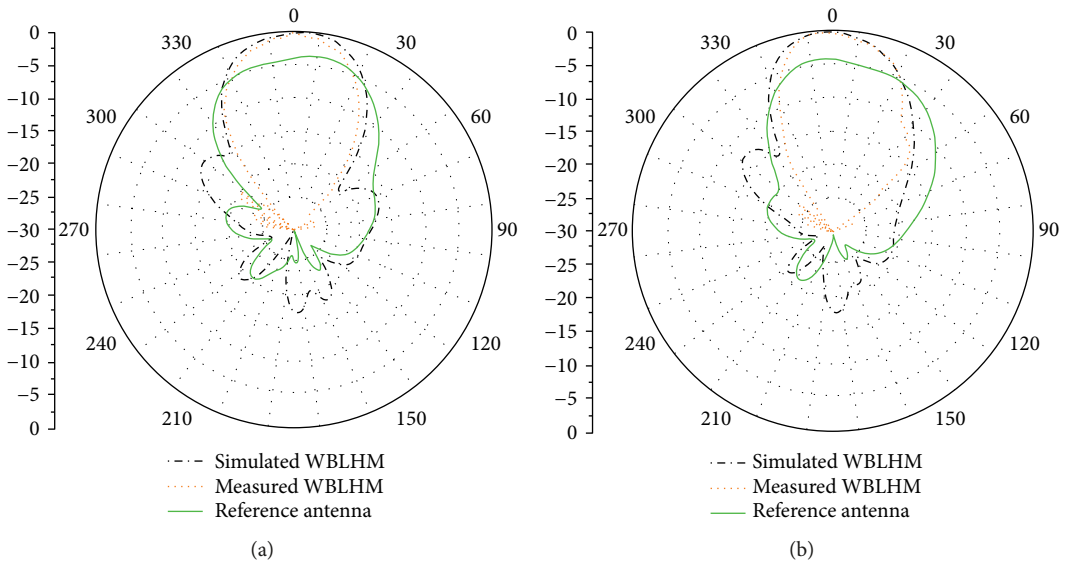

Figure 9: (a) Radiation pattern of reference antenna with and without WBLHM layer at 5.82 Ghz: (E-plane). (b) Radiation pattern of reference antenna with and without WBLHM layer at 5.82 Ghz (H-plane).

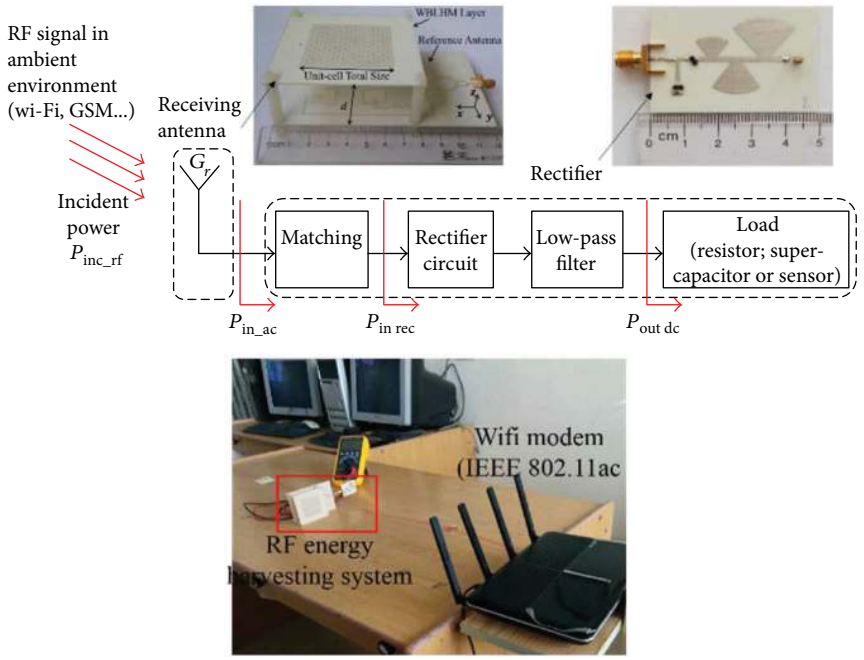

Figure 10: Wi-Fi energy harvesting system using WB CP LHM antenna.

4. Wideband CP LHM Antenna for RF Energy Harvesting

This proposed antenna is used as the receiving antenna for Wi-Fi energy harvester as shown in Figure 10.

The Schottky diode HSMS2860 from Avago is selected for the voltage doubler circuit. The configuration and prototype of this rectifier circuit is illustrated in Figure 10. The DC filter uses three radial stubs to reject the first-, second-, and third-order harmonic in order to improve conversion efficiency. The RF power transmitted by Wi-Fi modem based on IEEE 802.11ac standard is received by wideband CP LHM antenna and then converted into 1.5 DC voltage by the rectifier using the load of 3.9 kΩ. The simulated and measured $|S_{11}|$ of rectifier circuit are well match together (cf. Figure 11). The $|S_{11}|$ of rectifier is lower than −10 dB between 5.6 GHz to 5.9 GHz (in simulation) and between 5.55 GHz to 6.0 GHz (in measurement).

Figure 12(a) presents the conversion efficiency at different input power levels. The output voltage of RF-DC device is shown in Figure 12(b). The maximum conversion efficiency and corresponding input power level of RF-DC is

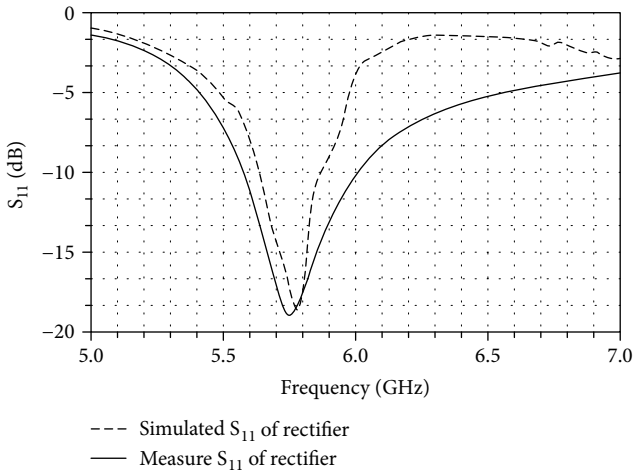

Figure 11: The simulated and measured S_{11} of rectifier.

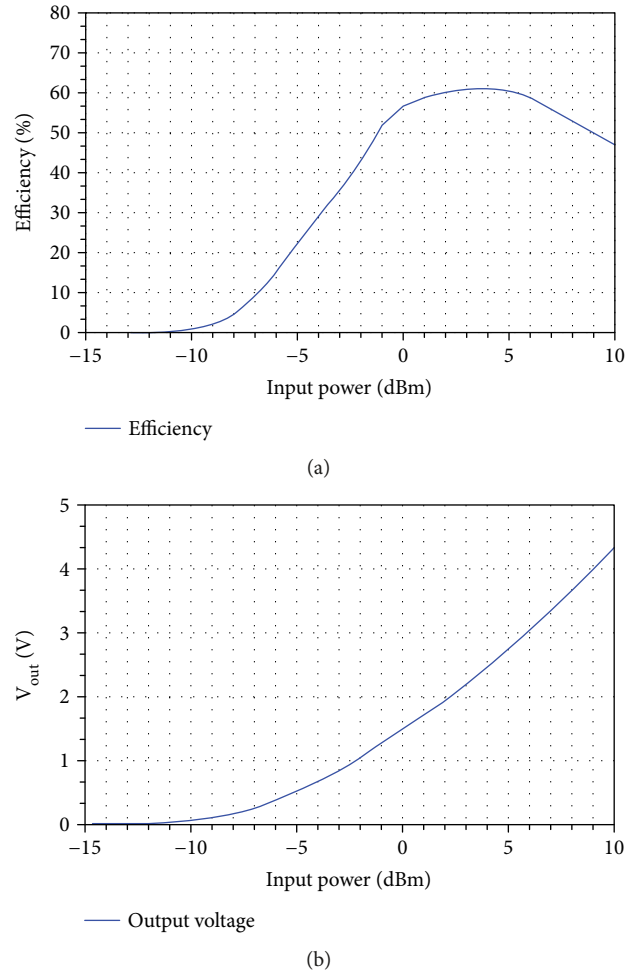

Figure 12: (a) RF-DC conversion efficiency versus input power level at 5.82 Ghz with the load of 3.9 kΩ. (b) Voltage output versus input power level at 5.82 Ghz with the load of 3.9 kΩ.

61% at 4 dBm with output voltage of 2.5 V. It can be seen that the output voltage is increasing with the increase of input power level. However, for the ambient RF energy harvesting application, the input power level is low, from 5 dBm or 0 dBm and less (−20 dBm), dependence on the RF sources (2G/3G/4G or Wi-Fi). The RF-DC device has conversion efficiency of 56% and output voltage of 1.5 V with input power level of 0 dBm using receiving antenna gain of 10.8 dBi at 5.82 GHz. In other experimentations, the RF-DC device uses the same rectifier circuit as presented in Figure 10 and a quasi-omnidirectional antenna with gain peak of 4 dBi as the receiving antenna. With input power level of 0 dBm, at the same frequency of Wi-Fi based on IEEE 802.11ac, the output voltage of 1.25 V is obtained instead of 1.5 V when using wideband CP LHM antenna. This result shows the advantages of proposed antenna in RF-DC application.

5. Conclusions

A novel WBLHM structure is proposed to enhance antenna performance in this paper. The behaviours of WBLHM layer are discussed using simulated S-parameters. The performances of this WBLHM are verified in simulation and measurement by applying on a wideband CP patch antenna operating from 5.05 GHz to 7.45 GHz. A maximum gain enhancement of 7.02 dBi is obtained at 6.15 GHz. A good performance for gain, AR, bandwidth, and total radiation efficiency is obtained from 5.8 GHz to 6.8 GHz using this wideband CP LHM antenna.

The application of wideband CP LHM antenna for Wi-Fi energy harvester presents 61% of conversion efficiency and 2.5 V of DC output voltage. This WBLHM substrate can be beneficial for broadband RF energy harvesting or wireless power transfer applications and implemented in the future wireless sensor networks.

Conflicts of Interest

The authors declare that there are no conflicts of interest regarding the publication of this paper.

Acknowledgments

This research is funded by Ministry of Education and Training (MOET) under grant number B2015-01-93. The authors wish to thank all members of RF3I lab for their help during our measurement and experimentations.

References

[1] Y. Gao, W. Cheng, H. Zhang, and Z. Li, "Heterogeneous statistical QoS provisioning over wireless powered sensor networks," *IEEE Access*, vol. 5, pp. 7910–7921, 2017.

[2] N. A. Bhatti, M. H. Alizai, A. A. Syed, and L. Mottola, "Energy harvesting and wireless transfer in sensor network applications: concepts and experiences," *ACM Transactions on Sensor Networks*, vol. 12, no. 3, pp. 1–40, 2016.

[3] W. C. Brown, "The history of power transmission by radio waves," *IEEE Transactions on Microwave Theory and Techniques*, vol. 32, no. 9, pp. 1230–1242, 1984.

[4] C. R. Valenta and G. D. Durgin, "Harvesting wireless power: survey of energy-harvester conversion efficiency in far-field,

wireless power transfer systems," *IEEE Microwave Magazine*, vol. 15, no. 4, pp. 108–120, 2014.

[5] N. B. Carvalho, A. Georgiadis, A. Costanzo et al., "Wireless power transmission: R &D activities within Europe," *IEEE Transactions on Microwave Theory and Techniques*, vol. 62, no. 4, pp. 1031–1045, 2014.

[6] M. Mrnka, P. Vasina, M. Kufa, V. Hebelka, and Z. Raida, "The RF energy harvesting antennas operating in commercially deployed frequency bands: a comparative study," *International Journal of Antennas and Propagation*, vol. 2016, Article ID 7379624, 11 pages, 2016.

[7] L.-G. Tran, H.-K. Cha, and W.-T. Park, "RF power harvesting: a review on designing methodologies and applications," *Micro and Nano Systems Letters*, vol. 5, no. 1, p. 14, 2017.

[8] C. Song, Y. Huang, J. Zhou, and P. Carter, "Recent advances in broadband rectennas for wireless power transfer and ambient RF energy harvesting," in *2017 11th European Conference on Antennas and Propagation (EUCAP)*, pp. 341–345, Paris, France, France, 2017.

[9] S. B. Vignesh, Nasimuddin, and A. Alphones, "Circularly polarized strips integrated microstrip antenna for energy harvesting applications," *Microwave and Optical Technology Letters*, vol. 58, no. 5, pp. 1044–1049, 2016.

[10] X. Bao, K. Yang, O. O'Conchubhair, and M. J. Ammann, "Differentially-fed omnidirectional circularly polarized patch antenna for RF energy harvesting," in *2016 10th European Conference on Antennas and Propagation (EuCAP)*, pp. 1–5, Davos, Switzerland, 2016.

[11] L. B. K. Bernard, Nasimuddin, and A. Alphones, "AN e-shaped slotted-circular-patch antenna for circularly polarized radiation and radiofrequency energy harvesting," *Microwave and Optical Technology Letters*, vol. 58, no. 4, pp. 868–875, 2016.

[12] S. B. Vignesh, Nasimuddin, and A. Alphones, "Stubs-integrated-microstrip antenna design for wide coverage of circularly polarised radiation," *IET Microwaves, Antennas & Propagation*, vol. 11, no. 4, pp. 444–449, 2017.

[13] L. B. K. Bernard, Nasimuddin, and A. Alphones, "Teo-shaped slotted-circular-patch antenna for circularly polarized radiation and RF energy harvesting," *Microwave and Optical Technology Letters*, vol. 57, no. 12, pp. 2752–2758, 2015.

[14] J. Zhang, H.-c. Yang, and D. Yang, "Design of a new high-gain circularly polarized antenna for Inmarsat communications," *IEEE Antennas and Wireless Propagation Letters*, vol. 11, pp. 350–353, 2012.

[15] Z. C. Hao, X. Liu, X. Huo, and K. k. Fan, "Planar high-gain circularly polarized element antenna for array applications," *IEEE Transactions on Antennas and Propagation*, vol. 63, no. 5, pp. 1937–1948, 2015.

[16] J. Zhou, E. N. Economon, T. Koschny, and C. M. Soukoulis, "Unifying approach to left-handed material design," *Optics Letters*, vol. 31, no. 24, pp. 3620–3622, 2006.

[17] C. Caloz and T. Itoh, *Electromagnetic Metamaterials: Transmission Line Theory and Microwave Applications: The Engineering Approach*, John Wiley & Sons, Inc., Hoboken, NJ, USA, 2005.

[18] D. R. Smith, W. J. Padilla, D. C. Vier, S. C. Nemat-Nasser, and S. Schultz, "Composite medium with simultaneously negative permeability and permittivity," *Physical Review Letters*, vol. 84, no. 18, pp. 4184–4187, 2000.

[19] D. R. Smith, D. C. Vier, N. Kroll, and S. Schultz, "Direct calculation of permeability and permittivity for a left-handed metamaterial," *Applied Physics Letters*, vol. 77, no. 14, pp. 2246–2248, 2000.

[20] C. A. Balanis, *Advanced Engineering Electromagnetics*, Wiley, New York, 1989.

[21] D. R. Smith and J. B. Pendry, "Homogenization of metamaterials by field averaging (invited paper)," *Journal of the Optical Society of America B*, vol. 23, no. 3, pp. 391–403, 2006.

[22] R. Liu, T. J. Cui, D. Huang, B. Zhao, and D. R. Smith, "Description and explanation of electromagnetic behaviors in artificial metamaterials based on effective medium theory," *Physical Review E*, vol. 76, no. 2, article 026606, 2007Part 2, 2007.

[23] D. R. Smith, J. Gollub, J. J. Mock, W. J. Padilla, and D. Schurig, "Calculation and measurement of bianisotropy in a split ring resonator metamaterial," *Journal of Applied Physics*, vol. 100, no. 2, article 024507, 2006.

[24] A. M. Nicolson and G. F. Ross, "Measurement of the intrinsic properties of materials by time-domain techniques," *IEEE Transactions on Instrumentation and Measurement*, vol. 19, no. 4, pp. 377–382, 1970.

[25] J. Baker-Jarvis, E. J. Vanzura, and W. A. Kissick, "Improved technique for determining complex permittivity with the transmission/reflection method," *IEEE Transactions on Microwave Theory and Techniques*, vol. 38, no. 8, pp. 1096–1103, 1990.

[26] X. Chen, T. M. Grzegorczyk, B.-I. Wu, J. Pacheco, and J. A. Kong, "Robust method to retrieve the constitutive effective parameters of metamaterials," *Physical Review E*, vol. 70, no. 1, 2004.

[27] E. J. Wilkinson, "An N-way hybrid power divider," *IEEE Transactions on Microwave Theory and Techniques*, vol. 8, no. 1, pp. 116–118, 1960.

[28] M. Malathong, A. Sonsilphong, W. Panpradit, and N. Wongkasem, "Chiral metamaterial based circularly polarized microstrip antennas," in *2011 IEEE-APS Topical Conference on Antennas and Propagation in Wireless Communications*, pp. 898–901, Torino, Italy, 2011.

[29] A. Balanis, *Antenna Theory Analysis and Design*, John Wiley & Sons, 3rd edition, 2005.